

High-Performance Solution-Processable Flexible SnSe Nanosheet Films for Lower Grade Waste Heat Recovery

Nicolas Augustus Rongione, Man Li, Huan Wu, Huu Duy Nguyen, Joon Sang Kang, Boya Ouyang, Hongyan Xia, and Yongjie Hu*

Lower grade waste heat recovery near room temperature is limited due to multiple technology challenges including low efficiency, high cost, and scalability. Here, a low-cost and scalable solution process is reported to fabricate a nanostructured SnSe thin film, and a high thermoelectric performance near room temperature is demonstrated. This transport study reveals strong phonon scattering near the interfaces between SnSe nanosheets that introduces a large thermal boundary resistance and an ultralow thermal conductivity of $0.09 \text{ W m}^{-1} \text{ K}^{-1}$. Moreover, it is demonstrated that the SnSe thin film can be readily implemented on flexible plastic substrates and preserve the high thermoelectric performance over 1000 bending cycles. Together, this study demonstrates a low-cost and scalable approach to achieve high-performance flexible thin film energy harvesting devices to power electronics and sensors near room temperature.

The growing demand for energy continues to represent a dichotomy in the struggle against increasing greenhouse gas emissions. In this endeavor, research has shown that over 15 quadrillion Joules of this energy is lost as waste heat, and among which, 80% of the waste heat is lower grade, i.e., below 400 K.^[1–8] Despite that various approaches including traditional steam cycles, Kalina cycles, and organic Rankine cycles have already been implemented in various industries for mid- to high-grade waste heat recovery, resulting in millions of saved dollars over long-term operation, such efforts are not yet economical for lower grade waste heat.^[1–4] In addition, most current approaches are limited to recovering waste heat from hot-water based systems,^[9] while the opportunities and requirements for wide-spread recovery of lower grade waste heat can be highly specific based on the industry of interest. Despite that a variety of novel solutions rooted in nanotechnology have been

emerging in literature,^[7] such efforts continue to be primarily limited in applicability due to low efficiencies far below the thermodynamic limit.


On the other hand, thermoelectrics, a solid-state technology that directly converts between heat and electricity attracted decades of investigations and has been matured for applications in radioisotope thermoelectric generators and Peltier coolers. The benefits of using thermoelectric materials manifest in their reliability, low-maintenance, and no moving parts, but have thus far been limited from lower grade waste heat recovery applications due primarily to their low energy efficiency.^[10] Recent efforts have focused on and succeeded in improving thermoelectric

energy efficiency and identifying new records of thermoelectric materials. However, the peak performance and associated temperature range of operation for most thermoelectric materials such as SiGe,^[11] PbTe,^[12] Clathrates,^[13] skutterudites,^[14] CuSe,^[15] and Cu_2S are currently focused on high temperature applications,^[16] and retain limited efficiency at low temperatures, below 400 K. The efficiency of these materials indeed benefits with increased temperature, as defined through the

thermoelectric material figure of merit, $ZT = \frac{\sigma S^2}{\kappa} T$, where σ is the electrical conductivity, S is the Seebeck coefficient, κ is the thermal conductivity, and T is the average absolute temperature. The state of the art room temperature thermoelectric materials remain to be alloys of expensive bismuth telluride^[16–18] ($\text{Bi}_{0.5}\text{Sb}_{1.5}\text{Te}_3$ with $ZT = 1.86 \pm 0.15$ at 320 K), which continue to benefit from and improve in performance with the development of new techniques to modify and enhance the properties of the compound as needed, such as through solid-solution alloying,^[19] porosity control,^[20] band engineering,^[21] topological states,^[22,23] resonance states,^[24] and hierarchical micro- and nanostructuring.^[12] While commercialization of thermoelectric materials and devices in the waste heat recovery market is expected to rapidly expand with a material ZT around 2–3 (≈ 10 –15% Carnot efficiency) at room temperature, these values have previously only been accessible in lab-environments or at high temperatures.^[4,19,25–27] New materials and geometries have emerged that may rival these compounds in terms of both cost and performance, including tin selenide (SnSe) with a record high ZT of 2.6 at 923 K in the $Cmcm$ structural phase.

N. A. Rongione, M. Li, H. Wu, H. D. Nguyen, J. S. Kang, B. Ouyang, Dr. H. Xia, Prof. Y. Hu
 School of Engineering and Applied Science
 University of California, Los Angeles
 Los Angeles, CA 90095, USA
 E-mail: yhu@seas.ucla.edu

Dr. H. Xia
 State Key Laboratory for Mechanical Behavior of Materials
 Xi'an Jiaotong University
 Xi'an 710049, China

 The ORCID identification number(s) for the author(s) of this article can be found under <https://doi.org/10.1002/aelm.201800774>.

DOI: 10.1002/aelm.201800774

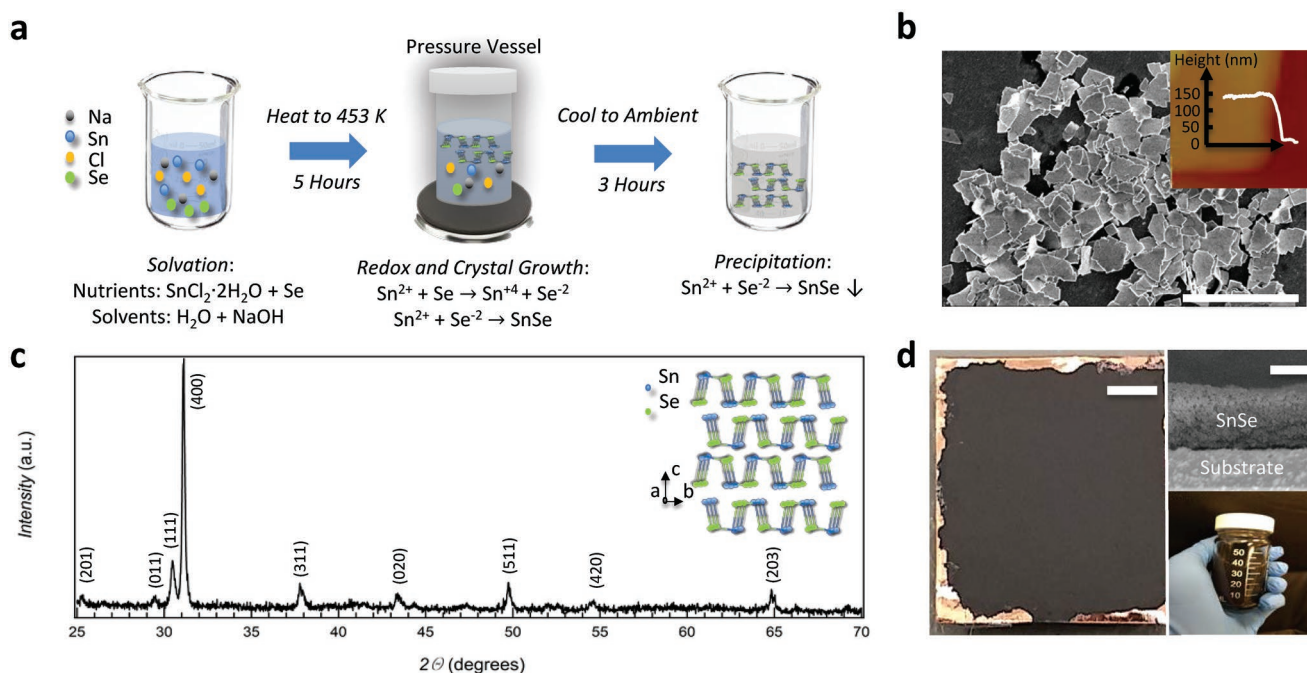


Figure 1. Chemical synthesis and structural characterization of tin selenide nanosheet stacks. a) Hydrothermal synthesis of tin selenide (SnSe) nanosheets using the hydrothermal method. b) Scanning electron microscopy (SEM) of as-synthesized SnSe nanomaterials, verifying it's in the form of nanosheets. The scale bar is 10 μm . Inset, atomic force microscopy (AFM) image showing the thickness of single SnSe nanosheet of about 100 nm. c) Powder X-ray diffraction (XRD) for SnSe with inset indicates its van der Waals crystal structure. d) Optical image of scaling up SnSe thin film, with the scale bar of 5 mm. The packed bed structure of the SnSe film is obtained from the scalable solution process (bottom right) and its cross-section is studied by SEM (top right with the scale bar of 50 μm).

This record thermoelectric performance has excited the field to try to understand its origin,^[28] and has led to a vast number of investigations that document its synthesis, characteristics, and applications.^[29–32] Moreover, SnSe has the highest reported device ZT from 300 to 773 K at ≈ 1.34 .^[33] Extensive efforts have begun to explore ways to tune doping to modulate and improve the performance of SnSe, including via the carrier concentration,^[27,33,34] and boundary scattering phenomena (nanostructuring),^[35,36] that can lower the thermal conductivity and maintain sufficient electrical conductivity. Structural control of SnSe has led to dramatic performance improvement and record-high efficiency, however, exploration of this new material for lower grade temperatures still lacks study.

Here, we report high-performance solution-processable flexible SnSe nanosheet stacks in a packed bed structure for lower grade waste heat recovery. The nanostructured SnSe in the morphology of 2D sheets are prepared using a readily scalable hydrothermal synthesis temperature difference method. The significant improvement over its bulk form is attributed to the largely reduced thermal conductivity due to interface phonon scattering. Furthermore, to evaluate the functional flexibility, SnSe samples are coated as a thin film on a flexible polyethylene terephthalate substrate with a bending test performed over 1000 cycles, showing highly stable performance for flexible energy harvesting devices.

We synthesized SnSe to achieve the structural form of 2D nanosheets using a surfactant-free hydrothermal synthesis method. In this method, nutrients in a sealed, hydrothermal autoclave reactor are dissolved in water-miscible solvents that

are heated for reaction. As detailed in **Figure 1a**, $\text{SnCl}_2 \cdot 2\text{H}_2\text{O}$ and NaOH are successively dissolved via sonication in a 50 mL beaker filled with deionized water (DI) water using 10 min sonication increments. By placing the reaction mixture on a preheated hot plate at 473 K for 5 h at 400 RPM, the high temperature and pressure thermodynamic conditions create a slurry of ions conducive for the reduction of the Se to Se^{2-} and oxidation of some of Sn^{+2} to Sn^{4+} , from which SnSe nanosheet crystals can begin to nucleate and grow in a process as described previously^[35,37] (Figure 1a). Note that the growth condition is designed to achieve a 2D surface morphology. Considering the law of Bravais,^[30,35,38–40] the morphology of the grown SnSe can be controlled by carefully selecting precursors and their concentrations to avoid suppression of the {001} and {010} higher surface energy planes in SnSe. In comparison, by utilizing a reaction pathway incorporating oleylamine surfactant, the [100] direction is only weakly suppressed to allow for growth of nanoflowers,^[39] versus in this paper where the growth along the [100] direction is strongly suppressed. Here, a 2D morphology of SnSe enhances surface contact areas and provides strong interfacial scattering events, from which a significant effect on the energy transport properties is expected. In the final reaction steps, the mixture is allowed to slowly return to ambient conditions under continued stirring to ensure limited particle aggregation as the newly synthesized particles precipitate out of the solution. The products are washed and collected using a decanting and gravitational sedimentation process that can capture the crystalline SnSe nanosheets. Finally, the nanosheets are redispersed into a suspension using DI water, sonication, and vortex mixing

before drop casting solutions; further details on the reaction and sample preparation are presented in the Supporting Information. Single SnSe nanosheets are carefully characterized using atomic force microscopy (AFM) (Figure 1b), showing a lateral dimension of about 3 μm and a thickness of about 150 nm.

Next, thin film of SnSe samples are prepared via drop casting for further characterizations. The crystalline structure of SnSe is determined by X-ray diffraction (XRD) shown in Figure 1c and confirmed to be orthorhombic *Pmna* space group 62 phase, whose crystal structure is illustrated in the inset of Figure 1c. Note that the solution processing method allows scaling nanomaterials for macroscopic device applications. As demonstrated in Figure 1d, a thin film of SnSe nanosheets was uniformly deposited using drop casting onto a copper tape substrate over an area of 1 cm^2 . A cross section scanning electron microscopy (SEM) of the sample details the high density of this packed bed structure, which is critical for thermoelectric transport.

To evaluate the potential for lower grade waste heat harvesting, the thermoelectric properties of the SnSe thin film in the cross-plane direction were measured near room temperature. The temperature gradient versus voltage gradient data are plotted in Figure 2a, indicating a p-type behavior of the SnSe film. Seebeck coefficient are measured for 300–400 K shown in Figure 2b, with room temperature value $S = 1250 \mu\text{V K}^{-1}$. As a control experiment, we also measured bulk SnSe single crystal samples synthesized by chemical vapor

deposition (see Supporting Information) and obtained a Seebeck coefficient of $809 \mu\text{V K}^{-1}$, consistent with literature.^[32] Note that the measured near-room temperature Seebeck of SnSe nanosheet films represents clear improvement over bulk single crystal SnSe, which was attributed to a possible carrier filtering effect from the high density of interfaces and low electrical conductivity as previously reported in SnSe nanostructures.^[32] Next, standard electrical transport measurement is performed across the SnSe nanosheet thin film. A linear I - V curve is measured in Figure 2c, indicating the Ohmic contact and an electrical conductivity of $\approx 2.4 \text{ S cm}^{-1}$ at 300 K. Figure 2d plots the temperature-dependent electrical conductivity, which exhibits semiconductor transport behavior: the conductivity decreases as temperature increases due to increased phonon scattering, and is consistent with undoped bulk SnSe.^[28] Note that the measured electrical conductivity of our SnSe nanosheet film is about 4.5 times lower than the single-crystal form.^[26] This reduced electrical conductivity is verified and expected as a compromise from the boundary scattering of electrons at the grain interfaces between the stacked nanosheets.

The thermal conductivity of SnSe thin film is measured using the hot-wire method.^[41] The hot-wire method is a standard technique for measuring a wide range of materials.^[41–46] In this method, a platinum wire is embedded in the SnSe powder, serving as both a line heat source and a temperature sensor, as depicted schematically in Figure 3a. After

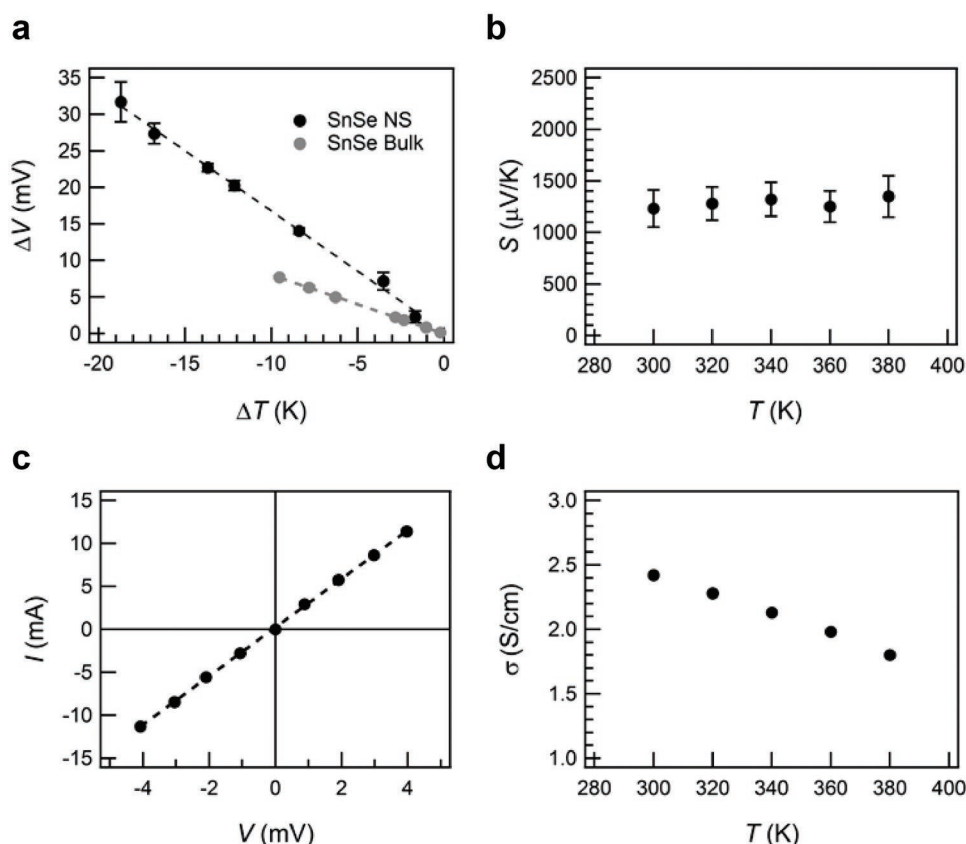


Figure 2. Seebeck and electrical characterization of the tin selenide thin film. a) Seebeck coefficient determination of tin selenide (SnSe) from 300 to 400 K, including nanosheets (NS, black) and bulk SnSe (gray) for comparison. b) Temperature-dependent Seebeck coefficient. c) Current–voltage transport curve. d) Temperature-dependent electrical conductivity.

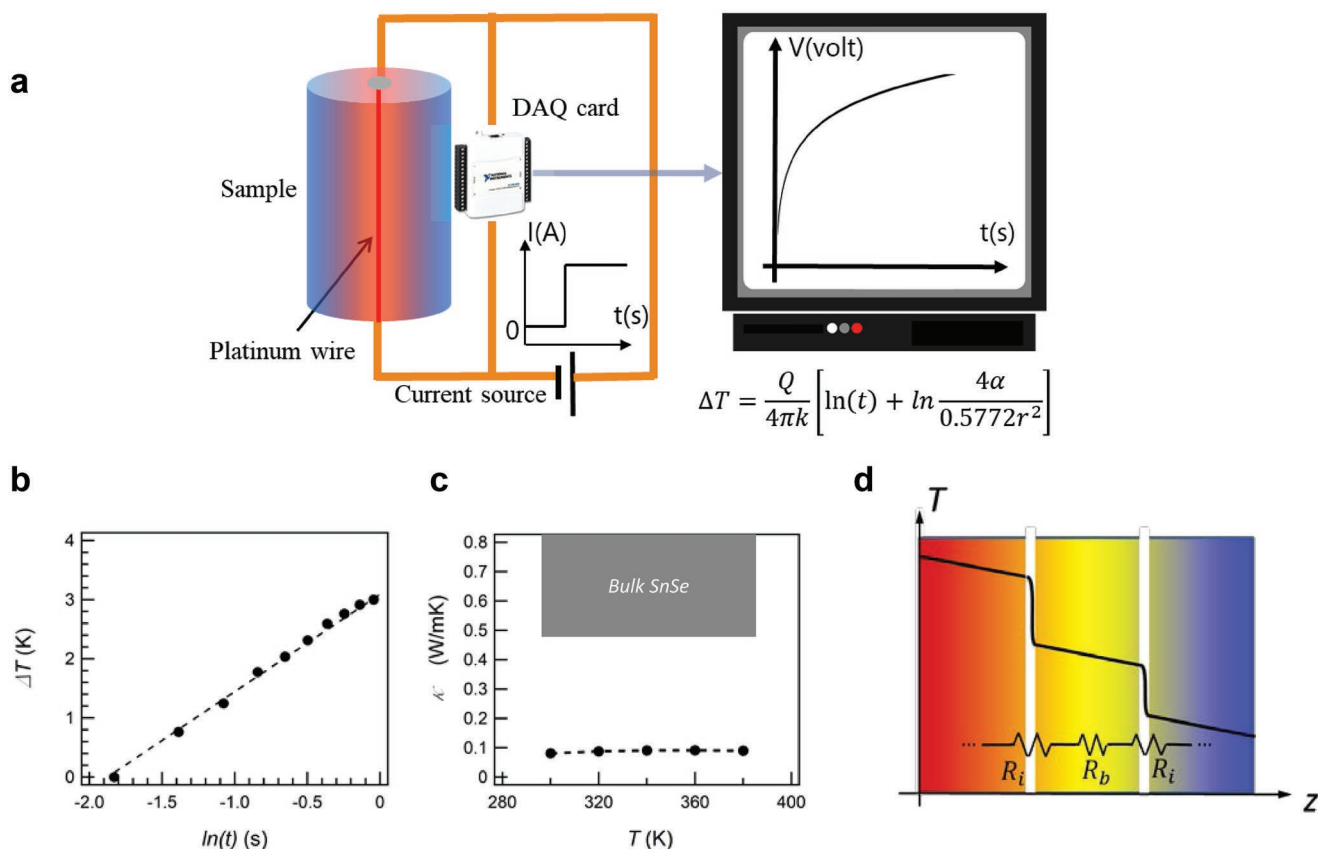


Figure 3. Thermal transport measurement and modeling of the tin selenide thin film. a) Schematic for hot-wire measurement. b) Typical measurement data and model fitting that determines the thermal conductivity. c) Temperature-dependent thermal conductivity, in comparison with bulk SnSe crystals. d) Schematic illustrating thermal boundary resistance and reduced effective thermal conductivity due to strong phonon scattering at the interfaces of SnSe nanosheets.

applying a constant current, uniform joule heating is generated along the wire. Using an infinitely large boundary condition and line heat source, the following heat conduction differential equation can be solved^[47]

$$T(r, t) = \frac{P}{4\pi kL} \left[\ln\left(\frac{4\alpha t}{r^2}\right) - \gamma \right] \quad (1)$$

where P is the Joule heating power, κ thermal conductivity, L length of the hot wire, α thermal diffusivity, t time, r the distance between wire center and interested point, and γ higher order terms regarding t and r , which can be neglected in our experiment. Thus, the thermal conductivity of the sample can be calculated from the slope of temperature rise versus the logarithmic value of time

$$\kappa = \frac{P}{4\pi L \cdot \text{slope}} \quad (2)$$

In our experiment, the temperature rise versus the logarithmic value of time is plotted in Figure 3b, and the temperature-dependent thermal conductivity is plotted in Figure 3c. While the thermal conductivity of single crystals is expected to decrease with an increase in temperature around room temperature,^[36] the thermal conductivity of SnSe films shows slight increase and indicates that the interface boundary

thermal conductance dominates the phonon transport in the nanostructures.^[48,49] Indeed, our experiment measures a very low cross-plane thermal conductivity $\kappa = 0.088 \pm 0.004 \text{ W m}^{-1} \text{ K}^{-1}$ for piled SnSe nanosheets at room temperature (Figure 3c), which is approximately seven times smaller than the intrinsic bulk thermal conductivity of single crystal SnSe.^[26,27]

We attribute such an ultralow thermal conductivity to the thermally resistive interfaces between nanosheets. In the thin film samples, individual SnSe nanosheets are piled together and form multiple interfaces which are expected to dominate the thermal resistance. To verify this expectation, a simplified multilayer model is built to estimate the interface thermal resistance R_i . The total thermal resistance through the entire material consists of two components: one is resistance due to the interface, and the other is resistance due to the intrinsic SnSe inside each individual nanosheet, i.e., the bulk crystal resistance. For n layers of SnSe nanosheets with thickness t for each layer, then the total thermal resistance R_{tot} through the whole material should be

$$R_{\text{tot}} = n \frac{t}{\kappa_{\text{exp}}} = n \frac{t}{\kappa_{\text{bulk}}} + nR_i \quad (3)$$

where κ_{bulk} and κ_{exp} are the thermal conductivity of the bulk single-crystal SnSe and the thermal conductivity of SnSe nanosheet measured by our experiment, respectively. The thickness of our

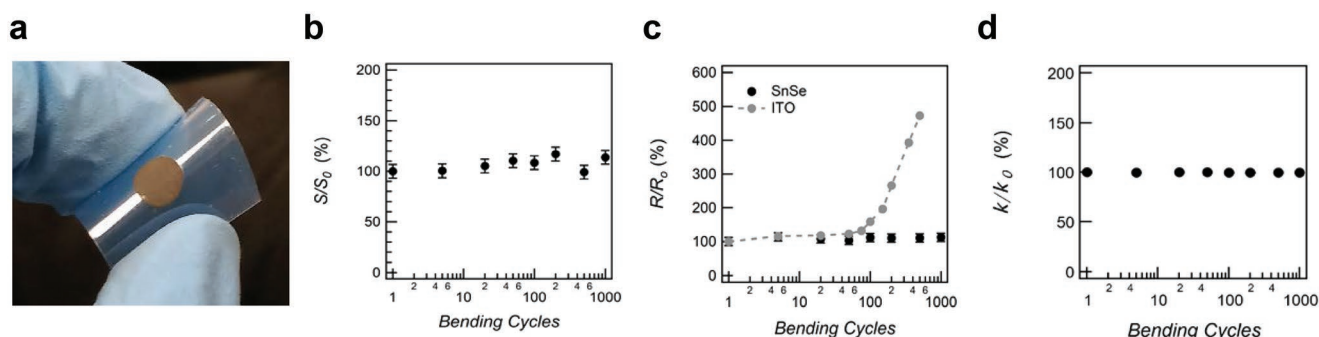


Figure 4. Thermoelectric performance of SnSe thin film on flexible substrate. a) Photograph of the SnSe thin film coated on a polyethylene terephthalate substrate under mechanical bending. b) Room-temperature relative change of the Seebeck coefficient S , c) electrical resistance R , and d) thermal conductivity κ of the thin film in response to the cyclic bending.

SnSe nanosheet is estimated to be 100 nm for this calculation. Based on Equation (3), the interface thermal resistance $R_i = 1.1 \times 10^{-6} \text{ m}^2 \text{ K W}^{-1}$. In comparison, the bulk thermal resistance is $3.3 \times 10^{-7} \text{ m}^2 \text{ K W}^{-1}$, more than three times smaller than R_i .

Hence, this large thermal boundary resistance dominates the overall contribution to the thermal conductivity of SnSe thin films. As illustrated in Figure 3d, the large thermal boundary resistance in the system leads to a large temperature drop at the interfaces and strong energy filter effects as expected. As a result of the largely reduced thermal conductivity, the SnSe nanosheet film provides high thermoelectric performance near 300 K. A high room-temperature ZT exceeding 1.2 has only been observed previously in quantum confinement structures such as atomically thin Bi_2Te_3 ^[50] and interface engineered bulk p-type $\text{Bi}_{0.5}\text{Sb}_{1.5}\text{Te}_3$ alloy.^[19]

As a further step, we fabricated the SnSe film on a flexible substrate and evaluated its promise as a building block for flexible energy harvesting devices. In Figure 4a, the SnSe is deposited on a polyethylene terephthalate substrate to demonstrate preserved functional material properties after being subjected to cyclic mechanical bending of the sample around a 4.5 mm radius of curvature surface. The bending cycle dependent Seebeck coefficient, electrical resistance, and thermal conductivity are plotted respectively in Figure 4b–d. As a control in Figure 4c, and to reference the severity of the prescribed bending regime, an indium tin oxide (ITO) film was subjected to the same bending configuration and its cycle dependent electrical resistance is measured for comparison. The ITO film begins to degrade dramatically between 100 to 1000 bending cycles, resulting in a five times increase in resistance. In contrast, the Seebeck coefficient, electrical resistance, and thermal conductivity of our SnSe sample maintain stable over 1000 bending cycles with a maximum fluctuation within 7%, 6%, and 5% respectively. The retention of the high-performance thermoelectric performance after mechanical bending underscore the promise of using SnSe nanostructures for powering flexible electronics and sensors on curved heating surfaces.

In summary, we have reported a high-performance thermoelectric thin film fabricated from a low-cost and scalable solution process for lower grade waste heat harvesting. The resulting SnSe nanosheet stacks introduces strong interface phonon scattering and exhibits an ultralow thermal conductivity of $0.09 \text{ W m}^{-1} \text{ K}^{-1}$ at room temperature, which are significantly lower than values of other polycrystalline forms reported in literature. Moreover, the SnSe thin film coated on

plastic substrate shows a superior flexibility and stability for integration with flexible electronics applications. The low-cost and scalable fabrication routes, together with the demonstrated high thermoelectric performance achieved in relatively earth-abundant materials, represents an important step in harvesting lower-grade waste heat and powering flexible electronic devices.

Supporting Information

Supporting Information is available from the Wiley Online Library or from the author.

Acknowledgements

Y.H. acknowledges support from a CAREER Award through the National Science Foundation, a Young Investigator Award through the US Air Force Office of Scientific Research, a PRF Doctoral New Investigator Award from the American Chemical Society, and the Sustainable LA Grand Challenge and the Anthony and Jeanne Pritzker Family Foundation. N.A.R acknowledges support from the National Science Foundation Graduate Research Fellowship under Grant No. 15–597.

Conflict of Interest

The authors declare no conflict of interest.

Keywords

2D van der Waals materials, energy efficiency, flexible electronics, nanostructures, phonons, solution-processing, thermal energy harvesting, thermoelectrics

Received: October 30, 2018

Revised: January 5, 2019

Published online: February 4, 2019

[1] The Energy Flow Chart Released by Lawrence Livermore National Laboratory, https://flowcharts.llnl.gov/content/assets/images/charts/energy/energy_2011_world.png (accessed: October 2011).

- [2] Geothermal Map of the United States, <https://www.Nrel.Gov/gis/geothermal.html> (accessed: October 2018).
- [3] I. Johnson, W. T. Choate, A. Davidson, *Waste Heat Recovery. Technology and Opportunities in US Industry*, BCS, Inc.: Laurel, MD, USA **2008**.
- [4] A. Thekdi, S. U. Nimbalkar, *Industrial Waste Heat Recovery-Potential Applications, Available Technologies and Crosscutting R&D Opportunities*, Oak Ridge National Laboratory (ORNL), Oak Ridge, TN, USA **2015**.
- [5] S. Chu, Y. Cui, N. Liu, *Nat. Mater.* **2017**, 16, 16.
- [6] S. Chu, A. Majumdar, *Nature* **2012**, 488, 294.
- [7] N. A. Rongione, H. Hguyen, H. Wu, Y. Hu, in *2017 IEEE 12th Int. Conf. on Nano/Micro Engineered and Molecular Systems (NEMS)*, IEEE, Los Angeles, CA, USA **2017**, pp. 826–831.
- [8] J. S. Kang, M. Li, H. Wu, H. Nguyen, Y. Hu, *Science* **2018**, 361, 575.
- [9] M. Langan, K. O'Toole, *Energy Procedia* **2017**, 123, 188.
- [10] M. S. Dresselhaus, G. Chen, M. Y. Tang, R. G. Yang, H. Lee, D. Z. Wang, Z. F. Ren, J.-P. Fleurial, P. Gogna, *Adv. Mater.* **2007**, 19, 1043.
- [11] J. Yang, T. Caillat, *MRS Bull.* **2006**, 31, 224.
- [12] K. Biswas, J. Q. He, I. D. Blum, C. I. Wu, T. P. Hogan, D. N. Seidman, V. P. Dravid, M. G. Kanatzidis, *Nature* **2012**, 489, 414.
- [13] M. Christensen, S. Johnsen, B. B. Iversen, *Dalton Trans.* **2010**, 39, 978.
- [14] X. Meng, Z. Liu, B. Cui, D. Qin, H. Geng, W. Cai, L. Fu, J. He, Z. Ren, J. Sui, *Adv. Energy Mater.* **2017**, 7, 1602582.
- [15] Z. Lin, C. Hollar, J. S. Kang, A. Yin, Y. Wang, H.-Y. Shiu, Y. Huang, Y. Hu, Y. Zhang, X. Duan, *Adv. Mater.* **2017**, 29, 1606662.
- [16] L. Yang, Z. G. Chen, M. S. Dargusch, J. Zhou, *Adv. Energy Mater.* **2018**, 8, 1701797.
- [17] T. Zhu, Y. Liu, C. Fu, J. P. Heremans, J. G. Snyder, X. Zhao, *Adv. Mater.* **2017**, 29, 1605884.
- [18] G. Homm, P. J. Klar, *Phys. Status Solidi RRL* **2011**, 5, 324.
- [19] S. I. Kim, K. H. Lee, H. A. Mun, H. S. Kim, S. W. Hwang, J. W. Roh, D. J. Yang, W. H. Shin, X. S. Li, Y. H. Lee, G. J. Snyder, S. W. Kim, *Science* **2015**, 348, 109.
- [20] B. Xu, T. Feng, M. T. Agne, L. Zhou, X. Ruan, G. J. Snyder, Y. Wu, *Angew. Chem.* **2017**, 129, 3600.
- [21] Y. Pei, H. Wang, G. J. Snyder, *Adv. Mater.* **2012**, 24, 6125.
- [22] Y. L. Chen, J. G. Analytis, J.-H. Chu, Z. K. Liu, S.-K. Mo, X. L. Qi, H. J. Zhang, D. H. Lu, X. Dai, Z. Fang, S. C. Zhang, I. R. Fisher, Z. Hussain, Z.-X. Shen, *Science* **2009**, 325, 178.
- [23] N. Xu, Y. Xu, J. Zhu, *npj Quantum Mater.* **2017**, 2, 51.
- [24] J. P. Heremans, B. Wiendlocha, A. M. Chamoire, *Energy Environ. Sci.* **2012**, 5, 5510.
- [25] C. B. Vining, *Nat. Mater.* **2009**, 8, 83.
- [26] L. D. Zhao, S. H. Lo, Y. Zhang, H. Sun, G. Tan, C. Uher, C. Wolverton, V. P. Dravid, M. G. Kanatzidis, *Nature* **2014**, 508, 373.
- [27] C. Chang, M. Wu, D. He, Y. Pei, C.-F. Wu, X. Wu, H. Yu, F. Zhu, K. Wang, Y. Chen, L. Huang, J.-F. Li, J. He, L.-D. Zhao, *Science* **2018**, 360, 778.
- [28] L.-D. Zhao, C. Chang, G. Tan, M. G. Kanatzidis, *Energy Environ. Sci.* **2016**, 9, 3044.
- [29] Z.-G. Chen, X. Shi, L.-D. Zhao, J. Zou, *Prog. Mater. Sci.* **2018**, 97, 283.
- [30] S. Weiran, G. Minxuan, W. Jinping, G. Jianfeng, F. Chenwei, A. Eric, L. Handong, W. Zhiming, *Adv. Sci.* **2018**, 5, 1700602.
- [31] Y. Xiao, C. Chang, Y. Pei, D. Wu, K. Peng, X. Zhou, S. Gong, J. He, Y. Zhang, Z. Zeng, L.-D. Zhao, *Phys. Rev. B* **2016**, 94, 125203.
- [32] D. Ibrahim, J.-B. Vaney, S. Sassi, C. Candolfi, V. Ohorodniichuk, P. Levinsky, C. Semprimoschnig, A. Dauscher, B. Lenoir, *Appl. Phys. Lett.* **2017**, 110, 032103.
- [33] L.-D. Zhao, G. Tan, S. Hao, J. He, Y. Pei, H. Chi, H. Wang, S. Gong, H. Xu, V. P. Dravid, C. Uher, G. J. Snyder, C. Wolverton, M. G. Kanatzidis, *Science* **2016**, 351, 141.
- [34] M. Gharsallah, F. Serrano-Sánchez, N. M. Nemes, F. J. Mompeán, J. L. Martínez, M. T. Fernández-Díaz, F. Elhalouani, J. A. Alonso, *Sci. Rep.* **2016**, 6, 26774.
- [35] C.-H. Chien, C.-C. Chang, C.-L. Chen, C.-M. Tseng, Y.-R. Wu, M.-K. Wu, C.-H. Lee, Y.-Y. Chen, *RSC Adv.* **2017**, 7, 34300.
- [36] S. Liu, N. Sun, M. Liu, S. Sucharitakul, X. P. A. Gao, *J. Appl. Phys.* **2018**, 123, 115109.
- [37] G. Tang, Q. Wen, T. Yang, Y. Cao, W. Wei, Z. Wang, Z. Zhang, Y. Li, *RSC Adv.* **2017**, 7, 8258.
- [38] X.-H. Ma, K.-H. Cho, Y.-M. Sung, *CrystEngComm* **2014**, 16, 5080.
- [39] L. Li, Z. Chen, Y. Hu, X. Wang, T. Zhang, W. Chen, Q. Wang, *J. Am. Chem. Soc.* **2013**, 135, 1213.
- [40] D. D. Vaughn, S.-I. In, R. E. Schaak, *ACS Nano* **2011**, 5, 8852.
- [41] M. J. Assael, K. D. Antoniadis, W. A. Wakeham, *Int. J. Thermophys.* **2010**, 31, 1051.
- [42] D. Wen, Y. Ding, *J. Thermophys. Heat Transfer* **2004**, 18, 481.
- [43] J. J. Healy, J. J. de Groot, J. Kestin, *Physica B+C* **1976**, 82, 392.
- [44] L. C. Wei, L. E. Ehrlich, M. J. Powell-Palm, C. Montgomery, J. Beuth, J. A. Malen, *Addit. Manuf.* **2018**, 21, 201.
- [45] R. Zheng, J. Gao, J. Wang, G. Chen, *Nat. Commun.* **2011**, 2, 289.
- [46] D. W. Stops, *Nature* **1949**, 164, 966.
- [47] D. Zhao, X. Qian, X. Gu, S. A. Jajja, R. Yang, *J. Electron. Packag.* **2016**, 138, 040802.
- [48] E. Tsotsas, H. Martin, *Chem. Eng. Process.* **1987**, 22, 19.
- [49] V. Goyal, D. Teweldebrhan, A. A. Balandin, *Appl. Phys. Lett.* **2010**, 97, 133117.
- [50] F. Zahid, *R. Lake, Appl. Phys. Lett.* **2010**, 97, 212102.